ELECTRODYNAMICS
AND WAVE PROPAGATION

Numerical Electrodynamic Investigation
of the Interior 3D Problem of the Sestroretskii Cube

A. S. Godin, M. S. Matsayan, and K. N. Klimov

AO NPO Lianozovo Electromechanical Plant, Dmitrovskoe sh. 110, Moscow, 127411 Russia
e-mail: andrey.godin@gmail.com, const0@mail.ru

Abstract—The numerical modeling of the frequency characteristics of the Sestroretskii cube is performed. It is shown that the interior Sestroretskii cube exhibits the properties of a double waveguide T-branch. The hypothesis that signals propagate inside the Sestroretskii cube with the velocity that is the double light speed in vacuum is justified. The limitations of the spectrum of these signals are formulated.

INTRODUCTION

The exterior and interior Huygens cubes (Fig. 1) where the electromagnetic wave propagates along a single spatial coordinate are considered in works [1–3]. The structure where the electromagnetic wave propagates along three spatial coordinates (a peculiar 3D Huygens cube) was first considered by Sestroretskii in 1983. This structure is called the Sestroretskii cube [4–7]. In the Russian literature, the analysis method using the Sestroretskii cube is called the method of an impedance analogue of the electromagnetic space [5]. Later such a structure was considered by Johns [8]. In the western literature, the analysis method using the Johns cube was called the transmission line method (TLM). It was developed by Hoefer [9], Christopoulos

[10], Trenkič [11], and Russer [12]. In these works, the properties of the electromagnetic wave propagation were postulated. It is of interest to numerically modulate the above structures for verifying the postulates formulated in these works.

1. INVESTIGATION OF THE INTERIOR SESTRORETSKII CUBE

Consider cube *A* of the dimensions $1 \times 1 \times 1$ mm (Fig. 2). Cube *A* is filled with vacuum. A rectangular parallelepiped also filled with vacuum is attached to every facet of cube *A*. The bases of the rectangular parallelepipeds coincide with the facets of cube *A* and have the equal heights $h = 0.05$ mm. However, we want to calculate the properties of the investigated cube
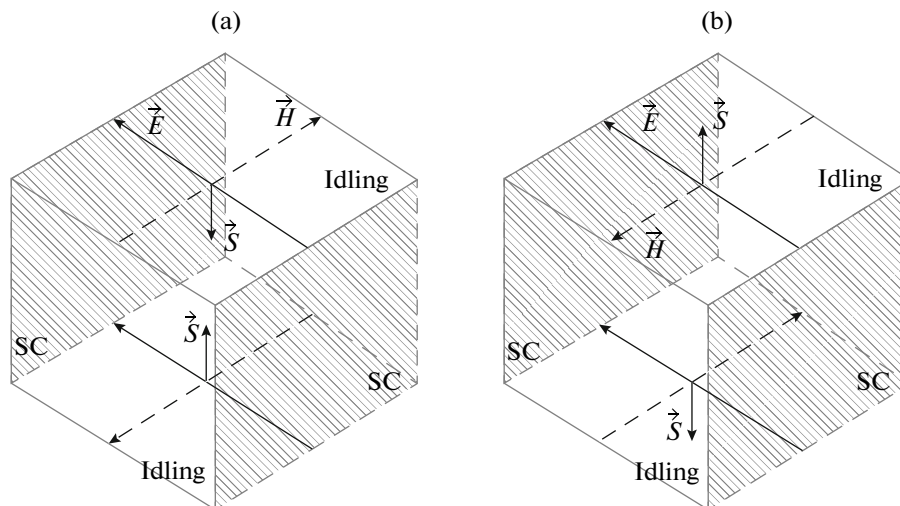

Fig. 1. (a) Interior and (b) exterior Huygens cubes where the electromagnetic wave propagation along one coordinate is illustrated.
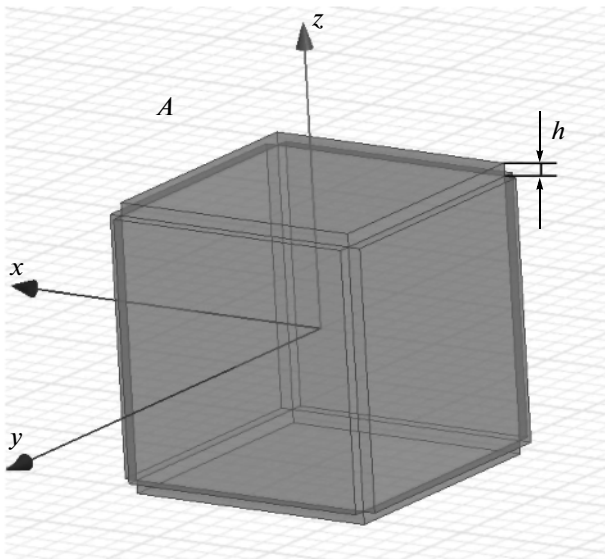
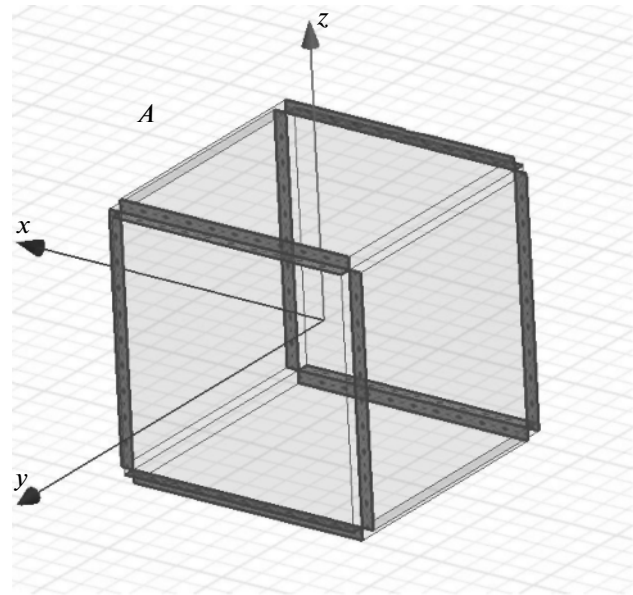**Fig. 2.** Geometry of cube A and rectangular parallelepipeds attached to its facets and filled with vacuum.

Fig. 3. Facets of rectangular parallelepipeds, on which the SC boundary condition is set.

when $h \to 0$. Therefore, after the numerical determination of the scattering matrix of the interior Sestroretskii cube with the help of code ANSYS HFSS v.15 [13], we move the reference planes of the inputs [14] of the device closely to cube A. In Fig. 2, height h is considerably smaller than the dimension of the edge of cube A. The number of rectangular parallelepipeds is six, which coincides with the number of facets of cube A. In Fig. 3, the facets of rectangular parallelepipeds connected to cube A are displayed. On these facets, we specify the boundary conditions for the tangential component of electric field E_τ, which is equal to zero. This corresponds to a metal wall. Consider that the facets of the cube are the short circuit (SC) walls [14−16].

In Fig. 4, the facets of rectangular parallelepipeds connected to cube A are marked out. On these facets, we specify the boundary conditions for the tangential components of magnetic field H_τ, which is equal to zero. This corresponds to a magnetic wall. Consider that the facets of this cube are the idling walls [14−16].

On all of the remaining facets of the rectangular parallelepipeds connected to cube A (Fig. 5), we specify the boundary conditions of excitation and matching of plane waves [14−16]. These conditions correspond to the inputs of the Sestroretskii cube. The input numeration is shown in Fig. 5. The polarizations of the intensities of the electric ($\vec{E}$) and magnetic ($\vec{H}$) fields and the directions of the vectors of Umov−Poynting energy flux densities $\vec{S}$ [17−20] for incident plane waves are shown in Fig. 6.

The considered geometry is a 3D interior Huygens cube, because it makes us possible to model the propagation of the electromagnetic wave along three spatial coordinates for interior problems of electromagnetics. This geometry was first considered by Sestroretskii in 1983. Therefore, we call it the interior Sestroretskii cube.

The scattering matrix of the interior Sestroretskii cube can be found from the scattering matrices of the cube halves in the cases of in-phase and antiphase excitations [4−8, 14].
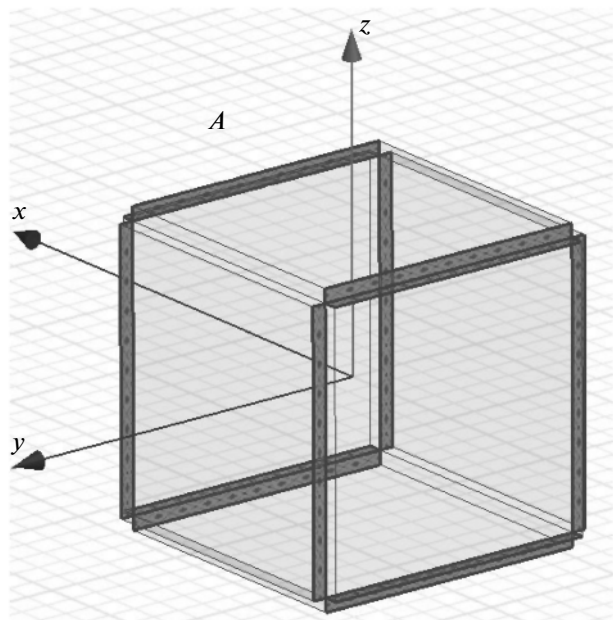

Fig. 4. Facets of rectangular parallelepipeds, on which the idling boundary condition is set.
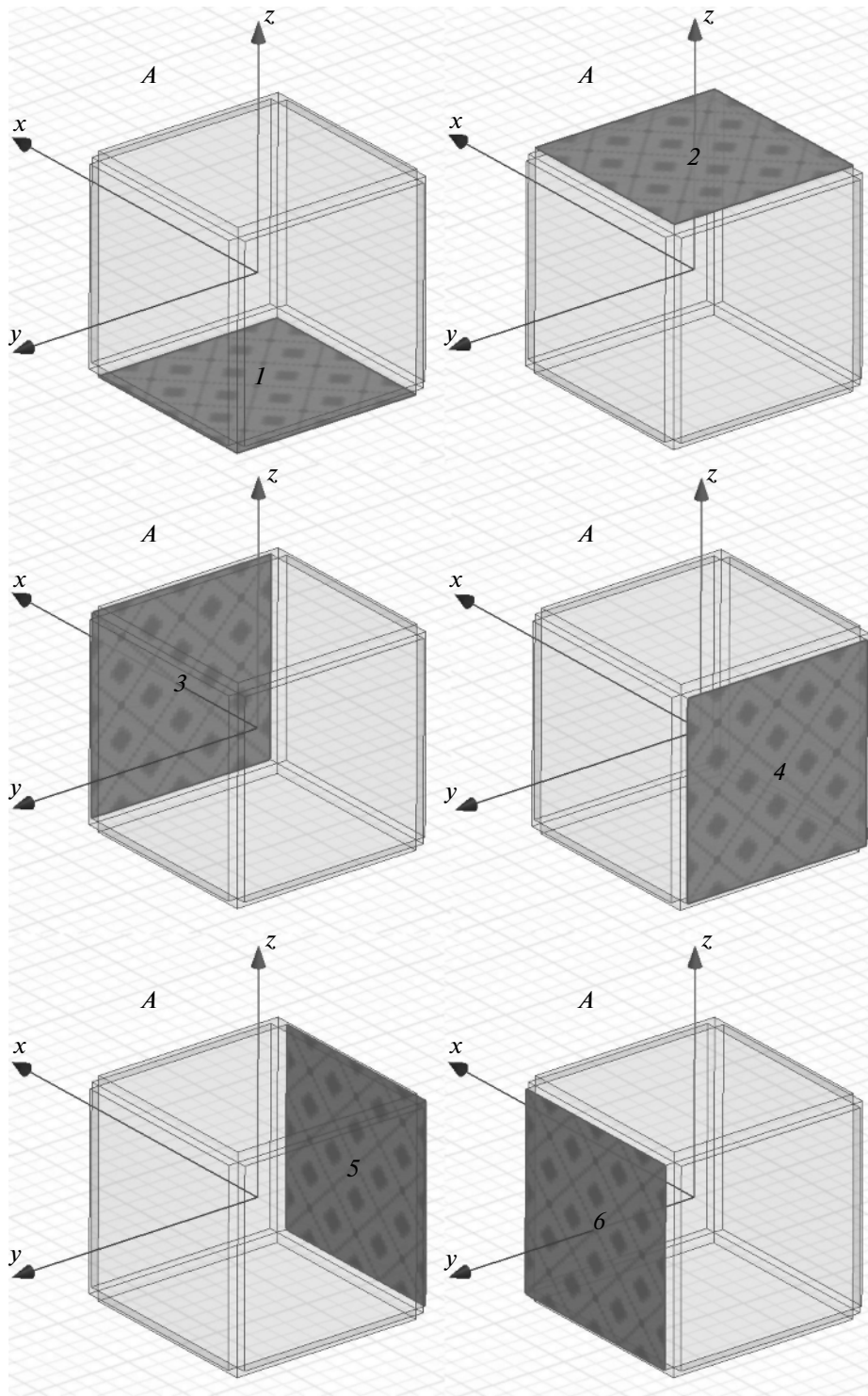
Fig. 5. Facets of rectangular parallelepipeds, which are connected to cube *A* and on which the boundary conditions for excitation and matching of plane waves are specified.
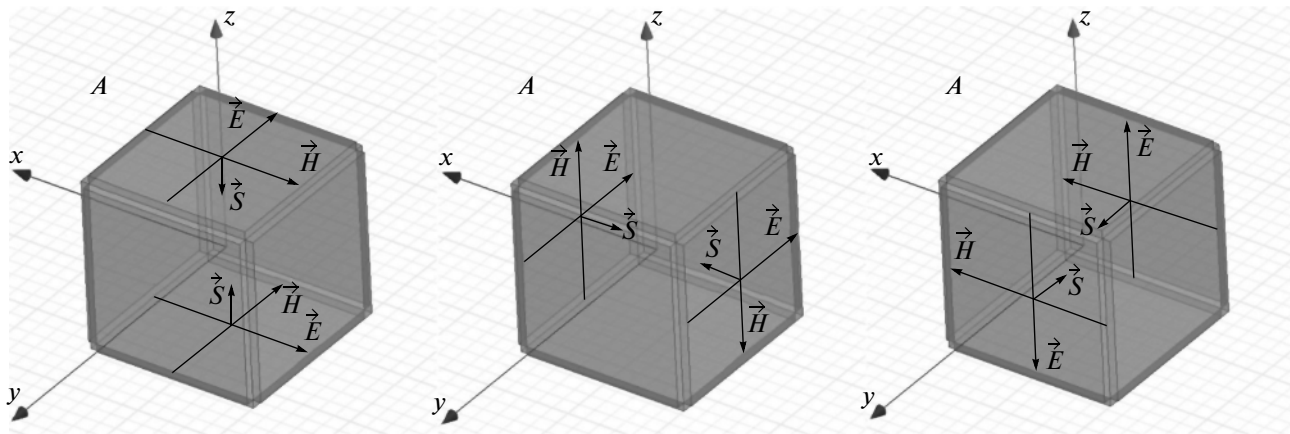
Fig. 6. Directions of the vectors of the electric ($\vec{E}$) and magnetic ($\vec{H}$) field intensities and the directions of the vectors of flux densities of electromagnetic (Umov−Poynting) field energies $\vec{S}$ for the waves incident on the inputs of the interior Sestroretskii cube.

2. THE INSIDE SESTRORETSKII CUBE IN THE PRESENCE OF THE IN-PHASE EXCITATION

Consider the interior Sestroretskii cube in the case when inputs *1* and *2* are in-phase excited (see Fig. 5). In the presence of this excitation the solution of the problem of scattering of the incident electromagnetic waves is equivalent to the solution of the problem for the geometry shown in Fig. 7. This geometry is the upper half of the initial geometry on whose lower facet the idling condition is given [4−7, 14]. We call this geometry the Sestroretskii cube half in the presence of the in-phase excitation (SCHIE) and denote it A^{++}.

The facets of the SCHIE where the idling conditions are set are shown in Fig. 8, and the facets of the SCHIE where the SC conditions are set are shown in Fig. 9. The inputs where the boundary conditions of matching and excitation of plane electromagnetic waves are given are enumerated in the same way as in the case of the initial geometry (see Fig. 5).

The SCHIE facets, where the boundary conditions of plane wave excitation and matching are given, are shown in Fig. 10 [14−16]. The polarizations of the intensities of the electric ($\vec{E}$) and magnetic ($\vec{H}$) fields and the directions of Umov−Poynting vectors $\vec{S}$ [17−20] of these plane waves are shown in Fig. 11.

Modeling of the problem of scattering of the SCHIE electromagnetic waves will be performed in the 3D electrodynamic code complex ANSYS HFSS v.15 [13].

3. RESULTS OF MODELING OF THE SESTRORETSKII CUBE HALF IN THE CASE OF THE IN-PHASE EXCITATION

The calculation is performed in the frequency range 1−300 GHz with a step of 1 GHs. The convergence of the modules of scattering matrix elements is Delta $S = 0.02$. The general number of tetrahedrons is 13352, the dimension of the obtained matrix is 83576, and 211 MB of RAM are used. The general time of the computation with the use of a computer having the Intel Core i7 processor with the frequency of 2.79 GHz and 12 GB of RAM is 59 min 04 s.

Figure 12 shows the frequency standing-wave ratio (SWR) characteristic for input *2* of the SCHIE. In the region of 1 GHz, the dimension of the SCHIE side is 1/300 of the wavelength, which is the quasi-static case.
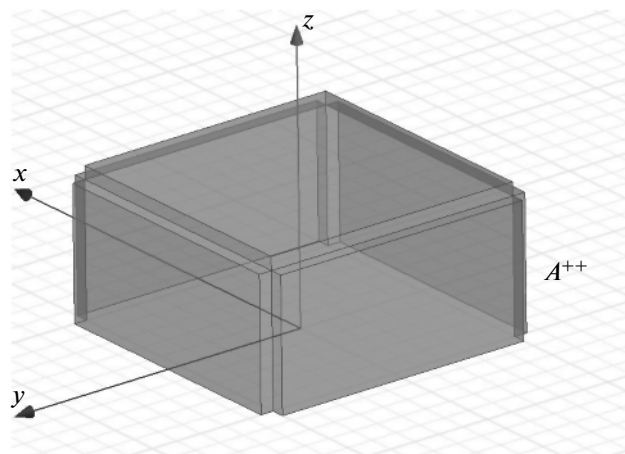

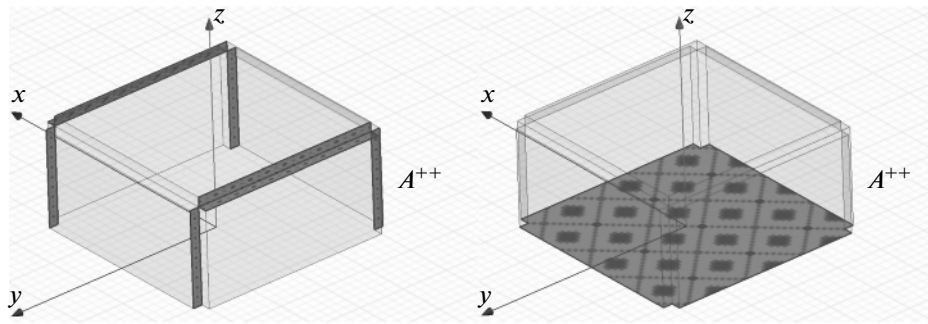**Fig. 7.** Geometry of SCHIE A^{++}.

Fig. 8. Geometry of SCHIE A^{++}, on which facets with the idling boundary condition are singled out.

The frequency characteristic of the SWR does not exceed 2 to the frequency of 131 GHz. At the frequency of 150 GHz (a half of the wavelength), we see the typical resonance, which is due to the possible propagation of waveguide modes H_{10} and H_{01} [21, 22]. In the interval 170−265 GHz, starting with 170 GHz, the quantity of the SWR frequency characteristic gradually grows from 2 to 3. At the frequency of 300 GHz, we observe one more resonance, which is due to the possible propagation of waveguide modes H_{20} and H_{02} [21, 22].

Figure 13 shows the possible frequency characteristic of the absolute value of reflection coefficient S for the SCHIE. It is seen from the figure that the reflection level is −74.46 dB at the frequency 1 GHz (1/300 of the wavelength). At the frequency of 150 GHz (a half of the wavelength), the reflection level decreases to −9.25 dB and gradually grows to 0 dB at the frequency of 300 GHz (the wavelength).

Figure 14 shows the frequency characteristic of attenuations when the signal passes from input *2* to input *3* (L_{23}, curve *1*) and from input *2* to input *4* (L_{24},

curve *2*) [14] for the SCHIE. It is seen from the figure that $L_{23} = L_{24}$ at all of the frequencies, which is evident from the symmetry properties. At the frequency 1 GHz (1/300 of the wavelength), the values of attenuations L_{23} and L_{24} are −3 dB, i.e., we can say that the signal arriving at input *2* is divided between inputs *3* and *4*. At the frequency of 150 GHz (the dimension of the SCHIE edge corresponds to a half of the wavelength), we see the characteristic resonance of the SCHIE and the values of L_{23} and L_{24} are −27.13 dB. At the frequency of 170 GHz, the frequency characteristic of attenuation again increases and is −6.34 dB. When the frequency continues to increase to 300 GHz, the values of attenuations L_{23} and L_{24} continue to decrease and are −41 and −39 dB, respectively.

Figure 15 shows the frequency characteristic of isolations J between inputs *2* and *5* (J_{25}, curve *1*) and inputs *2* and *6* (J_{26}, curve *2*) for the SCHIE. It is seen from the figure that, practically at all frequencies $J_{25} = J_{26}$, and, at the frequency of 1 GHz (when the dimension of the SCHIE edge corresponds to 1/300 of the wavelength), the values of J_{25} and J_{26} are −61.65 dB. At the frequency of 150 GHz (a half of the wavelength), we see the characteristic resonance of isolation J_{25} and J_{26} of the SCHIE, and the peak is −10.8 dB. The values of the isolations increase at the frequency of 170 GHz and are −6.22 dB. The isolations increase at the frequency 260 GHz to the values of J_{25} and J_{26}, which are equal to −4.6 dB. The values of J_{25} and J_{26} continue to decrease to 300 GHz and are −17.8 dB.

The frequency characteristic of phase φ of the coefficient of the transmission from input *2* to input *3* (curve *1*) and from input *2* to input *4* (curve *2*) for the SCHIE is given in Fig. 16. Because of the symmetry of the SCHIE geometry, the phases of the coefficient of the transmission from input *2* to input *3* and from input *2* to input *4* are equal at all frequencies, which is seen from Fig. 16. Note that φ radians should be subtracted from phase π of the reflection coefficient [1−3], because code ANSYS HFSS v.15 chooses the electric field polarization for the SCHIE inputs that has the
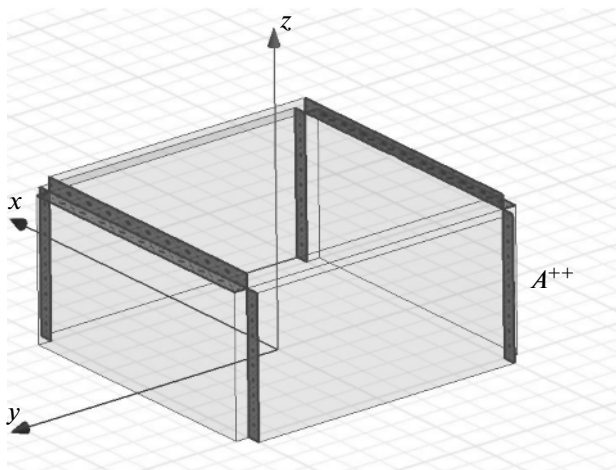

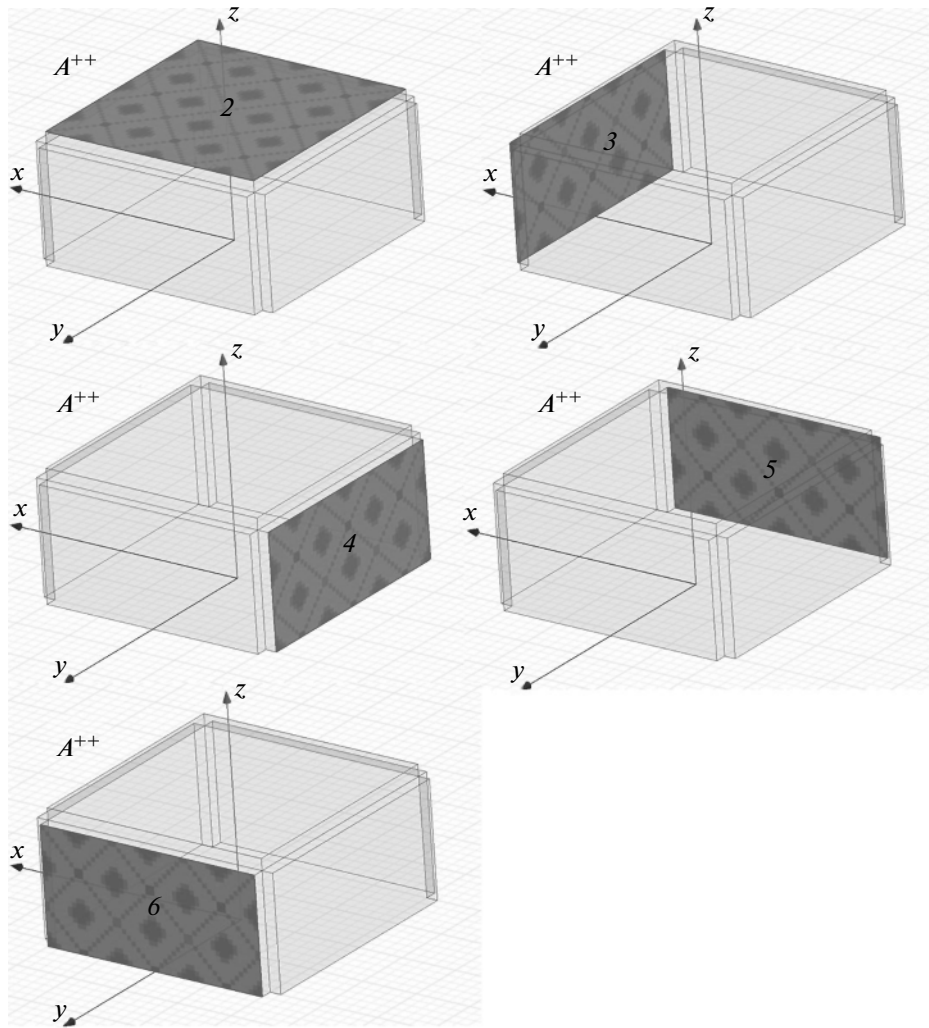**Fig. 9.** Geometry of SCHIE A^{++}, on which facets with the SC boundary condition are singled out.

Fig. 10. Facets of SCHIE A^{++}, on which the boundary conditions are specified for excitation and matching of plane waves.
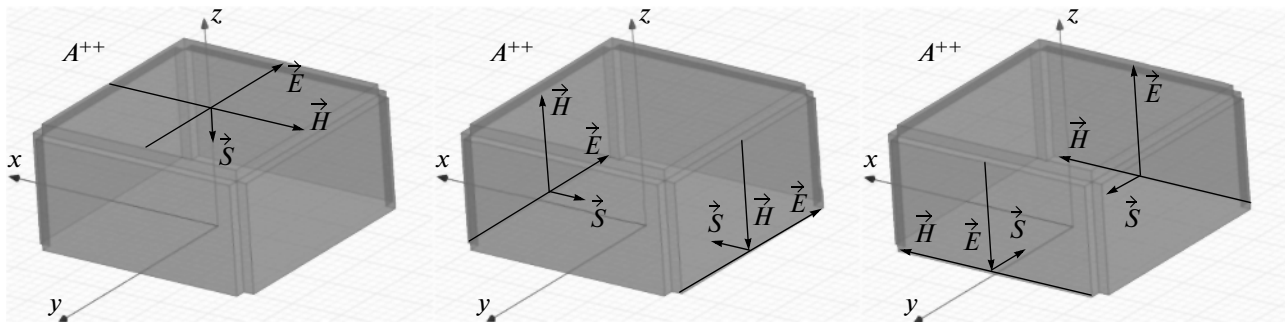
Fig. 11. Directions of the vectors of the electric ($\vec{E}$) and magnetic ($\vec{H}$) field intensities and the directions of the vectors of flux densities of electromagnetic (Umov−Poynting) field energies $\vec{S}$ for the waves incident on the inputs of SCHIE A^{++}.
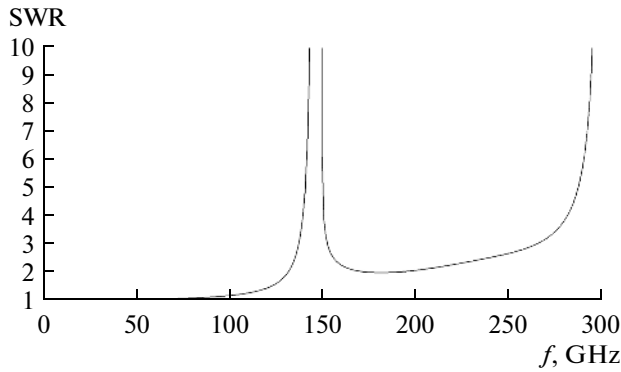
Fig. 12. Frequency characteristic of the SWR of the SCHIE for input *2* calculated in code ANSYS HFSS v.15.
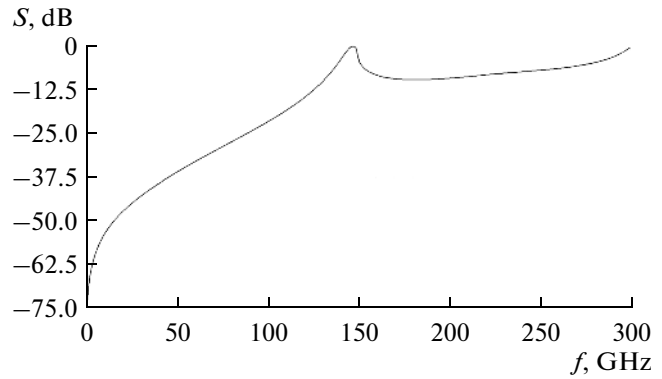

Fig. 13. Frequency characteristic of the absolute value of the reflection coefficient of the SCHIE for input *2* calculated in code ANSYS HFSS v.15.
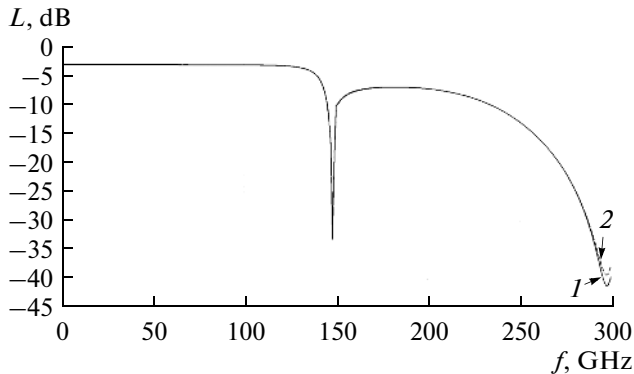

Fig. 14. Frequency characteristic of attenuations observed when the signal goes (L_{23}, curve *1*) from input *2* to input *3* and (L_{24}, curve *2*) from input *2* to input *4*. The characteristic is obtained for the SCHIE.
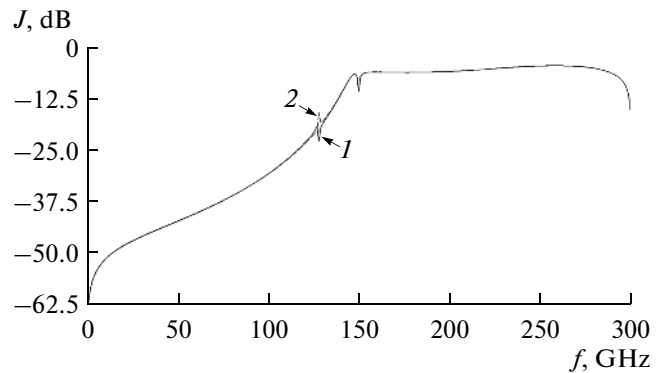

Fig. 15. Frequency characteristics of (curve *1*) isolation J_{25} between inputs *2* and *5* and (curve *2*) isolation J_{26} between inputs *2* and *6* for the SCHIE.

opposite direction as compared to the direction shown in Fig. 11.

The frequency characteristic (see Fig. 17) of the time delay estimation is based on the formulas

$$\Delta t_{23} = \frac{\arg(S_{23}) - \pi}{2\pi f}, \tag{1}$$

$$\Delta t_{24} = \frac{\arg(S_{24}) - \pi}{2\pi f}. \tag{2}$$

Here, Δt_{23} is the time delay (in seconds) between inputs *2* and *3*, Δt_{24} is the time delay (in seconds) between inputs *2* and *4*, $\arg(S_{23})$ is the phase (in radians) of the coefficient of transmission from input *2* to input *3* of the SCHIE, $\arg(S_{24})$ is the phase (in radians) of the coefficient of transmission from input *2* to input *4* of the SCHIE, and *f* is the frequency in hertzes.

It is seen from Fig. 17 that delay time *t* is estimated by 1.65 ps for inputs *3* and *4*. The characteristic reso-

nances of the delay time are seen at the frequency 150 GHz (the dimension of the SCHIE corresponds to the half of the wavelength) and at the frequency 300 GHz (the dimension of the SCHIE corresponds to the wavelength).

Figure 18 shows the plots of the frequency dependences of velocity v with which the signal goes from input *2* to input *3* and from input *2* to input *4* inside the SCHIE. For the SCHIE, velocity v of the signal passage relative to the light speed is calculated as follows:

$$v = \frac{10^{-3}}{\Delta t} \frac{1}{c}, \tag{3}$$

where 10^{-3} is the dimension of the SCHIE edge (in meters), Δt is the delay time (in seconds) of the signal passage corresponding to expression (1), and c is the light speed in vacuum (in meters per second).

It is seen from Fig. 18 that, at the frequency of 1 GHz, the relative value of the velocity with which the signal passes in the SCHIE is twice as large as the light
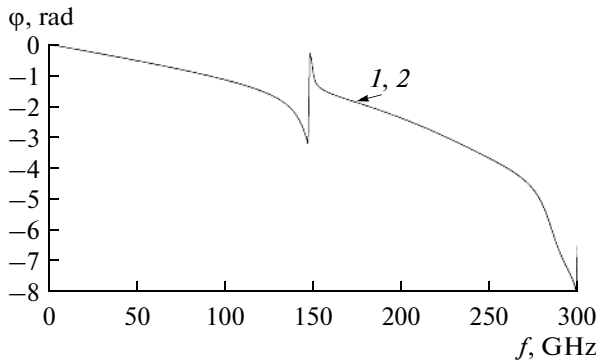
Fig. 16. Frequency characteristic of phase φ of the coefficient of transmission (curve *1*) from input *2* to input *3* and (curve *2*) from input *2* to input *4* for the SCHIE.
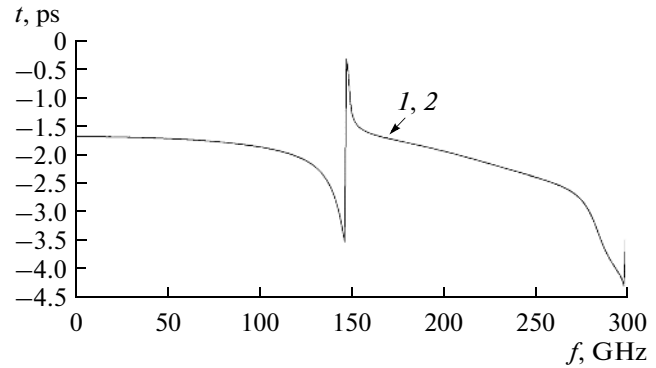

Fig. 17. Frequency characteristic of time delay estimate *t* for the signal propagating (curve *1*) from input *2* to input *3* and (curve *2*) from input *2* to input *4* for the SCHIE.
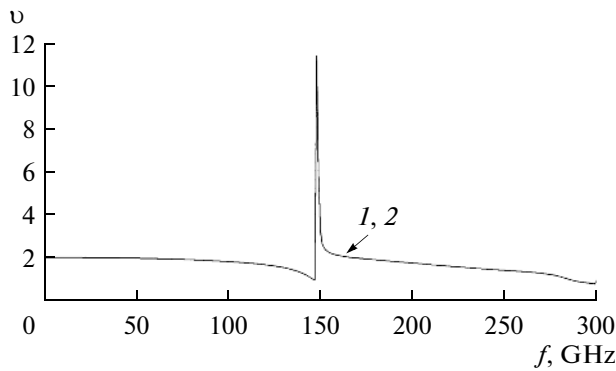

Fig. 18. Velocity of the signal propagating (curve *1*) from input *2* to input *3* and (curve *2*) from input *2* to input *4* for the SCHIE.
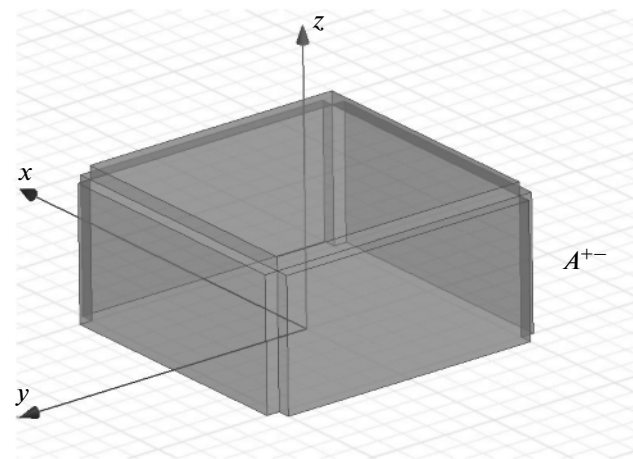

Fig. 19. Geometry of the HSCAE A^{+-}.

speed. After that, we observe the smooth decrease of the signal passage velocity to 0.96 of light speed *c* at the frequency of 147 GHz. The characteristic resonances of the signal transmission velocity are seen at the frequencies 150 and 300 GHz.

Thus, the frequency characteristics of the SCHIE calculated with the help of code ANSYS HFSS v.15 are considered.

4. THE INTERIOR SESTRORETSKII CUBE IN THE PRESENCE OF THE ANTIPHASE EXCITATION

Consider the interior Sestroretskii cube for antiphase excitation of inputs *1* and *2* (see Fig. 5). In the case of this excitation, the solution of the problem about scattering of incident electromagnetic waves is equivalent to the solution of the problem for the geometry shown in Fig. 19. This geometry is the upper half of the initial geometry on whose lower facet the SC

condition is set [4−7, 14]. We call this geometry the half of the Sestroretskii cube for antiphase excitation (HSCAE) and denote it A^{+-}.

Figure 20 shows the HSCAE facets where the idling boundary conditions are set, and Fig. 21 shows the HSCAE facets where the SC boundary conditions are set. The enumeration of inputs where the boundary conditions for matching and excitation of electromagnetic waves are set is the same as that on the original geometry (see Fig. 5).

Figure 22 shows the HSCAE facets where the boundary conditions for excitation and matching of plane waves are set [14−16]. The polarizations of the electric ($\vec{E}$) and magnetic ($\vec{H}$) field intensities and the directions of Umov−Poynting vectors $\vec{S}$ [17−20] of these plane waves are shown in Fig. 23.

Modeling of the problem of scattering of HSCAE electromagnetic waves will be performed in the 3D electrodynamic code complex ANSYS HFSS v.15 [13].
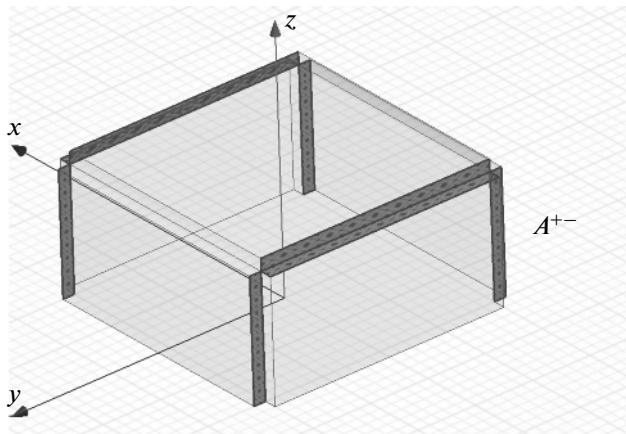
Fig. 20. Geometry of the HSCAE A^{+-}, where the facets with the idling boundary condition are marked out.

5. RESULTS OF MODELING OF THE HALF OF THE SESTRORETSKII CUBE FOR ANTIPHASE EXCITATION

The geometry of the HSCAE is dual [21] to the geometry of the SCHIE when the first one is turned by 90° around the z axis. Therefore, the frequency characteristics of the SWR, attenuation, isolation, the phases of the transmission coefficient, the delay time, and the relative velocity of the signal delay for the HSCAE (see Figs. 12–18) are the same as for the SCHIE for the following replacement of the input enumeration: input *2* of the SCHIE corresponds to input *2* of the HSCAE, input *3* of the SCHIE corresponds to input *5* of the HSCAE, input *5* of the SCHIE corresponds to input *4* of the HSCAE, input *4* of the SCHIE corresponds to input *6* of the HSCAE, and input *6* of the SCHIE corresponds to input *3* of the HSCAE. Therefore, it is not necessary to perform the calculation.

The full matrix of scattering of the Sestroretskii cube is found on the basis of the scattering matrices of

the SCHIE and HSCAE according to the method from [4–7, 14].

6. RESULTS OF MODELING OF THE SESTRORETSKII INTERIOR CUBE

We present the results for the frequency characteristics of the full interior Sestroretskii cube.

The plots of the frequency characteristics of the SWR and the absolute value of the reflection coefficient for input *2* of the interior Sestroretskii cube coincide with the corresponding frequency characteristics for the SCHIE (see Figs. 12 and 13).

The frequency characteristic of the dependences of the coefficient of transmission from input *2* to inputs *3–6* (curves *1–4*) of the interior Sestroretskii cube is shown in Fig. 24. For comparison, the frequency characteristic of the dependences of the coefficient of transmission from input *2* to inputs *3* and *4* (curves *5* and *6*) for the SCHIE is also shown. It is seen from the figure that the plots of the frequency dependence of the coefficient of transmission from input *2* to inputs *3–6* and from input *2* to inputs *3* and *4* coincide. This follows from the symmetry properties. At the frequency of 1 GHz (the dimension of the edge of the interior Sestroretskii cube corresponds to 1/300 of the wavelength), the values of the transmission coefficient for the interior Sestroretskii cube are equal to −6 dB. This value remains up to the frequency 120 GHz. Note that the size of the edge of the interior Sestroretskii cube corresponds to 2/5 of the wavelength. At the frequency of 150 GHz (when the size of the edge of the interior Sestroretskii cube corresponds to the half of the wavelength), the characteristic resonance of the interior Sestroretskii cube is seen and the values of the transmission coefficient are −31.21 dB. After that, the value of the transmission coefficient for the Sestroretskii cube grows and, at the frequency 280 GHz, is −9.22 dB. At the frequency 300 GHz, the value of the coefficient of the Sestroretskii cube transmission is −21.41 dB.

As we see, up to the half of the wavelength, when higher mode types do not start propagating, the behav-
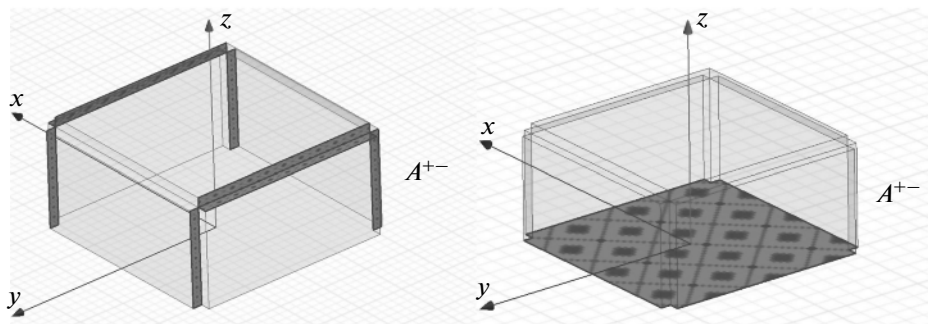

Fig. 21. Geometry of the HSCAE A^{+-}, where the facets with the SC boundary condition are marked out.

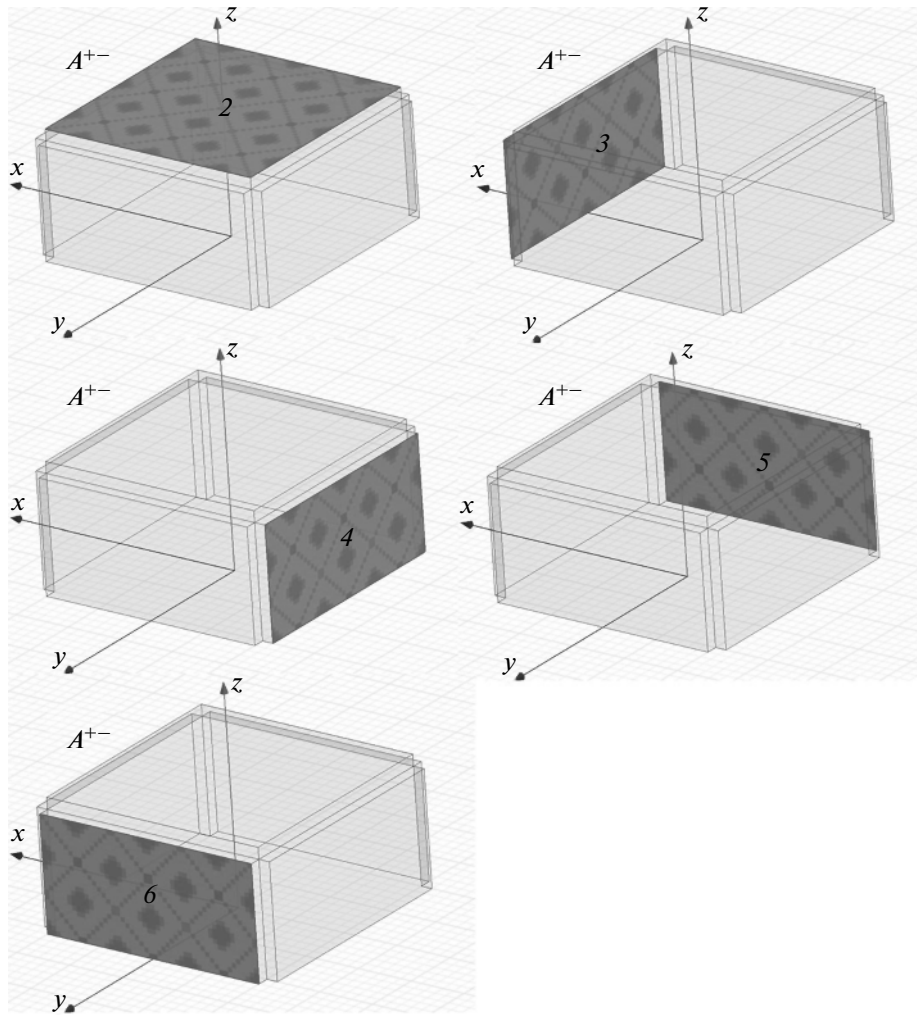**Fig. 22.** Facets of the HSCAE A^{+-}, on which the boundary conditions are specified for excitation and matching of plane waves.
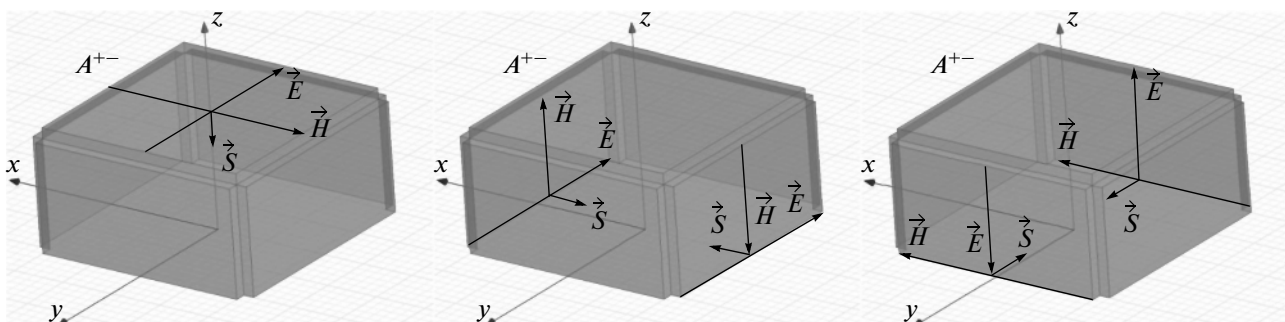

Fig. 23. Directions of the vectors of the electric ($\vec{E}$) and magnetic ($\vec{H}$) field intensities and the directions of the vectors of flux densities of electromagnetic (Umov−Poynting) field energies $\vec{S}$ for the waves incident on the inputs of HSCAE A^{+-}.
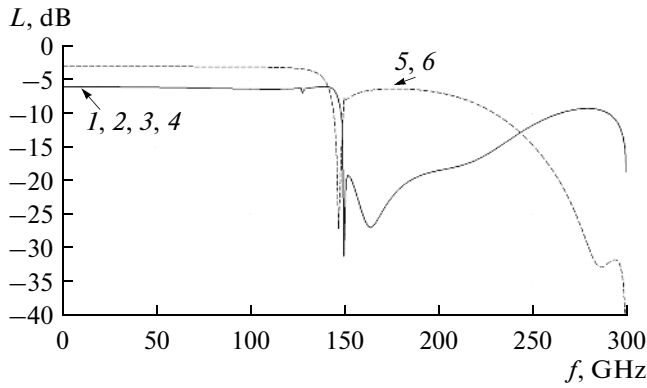
Fig. 24. Frequency characteristic of coefficient L of transmission (curves 1–4) from input 2 to inputs 3–6 of the interior Sestrortskii cube and (curves 5 and 6) from input 2 to inputs 3 and 4 for the SCHIE.

ior of the transmission coefficient for the interior Sestroretskii cube corresponds to the behavior of the SCHIE transmission coefficient, and their values are different by 3 dB. This is clear, because, for the SCHIE, the energy arriving at input 2 is divided between two inputs: 3 and 4, and, for the interior Sestroretskii cube, the energy arriving at input 2 is divided between four inputs: 3–6. Up to the frequency of 120 GHz, the isolation value between SCHIE inputs 2, 5, and 6 is −25 dB (see Fig. 15). For the frequencies exceeding 120 GHz, the absolute value of the above isolation is reduced. In addition, after 150 GHz, the waveguide modes start propagating, and, therefore, the behavior of the transmission coefficient for the interior Sestroretskii cube does not coincide with the behavior of the transmission coefficient for the SCHIE.

The frequency characteristic of phase φ of the coefficient of transmission from input 2 to inputs 3–6 (curves 1–4) for the interior Sestroretskii cube is given

in Fig. 25. For comparison, we also show the frequency characteristic of phase φ of the coefficient of the signal transmission from input 2 to inputs 3 and 4 (curves 5 and 6) for the SCHIE. It is seen from Fig. 25 that the phases of the coefficient of the signal transmission from input 2 to inputs 3–6 are equal at all of the frequencies because of the symmetry of the geometry of the interior Sestroretskii cube.

Up to the frequency 90 GHz (when the size of the edge of the interior Sestroretskii cube corresponds to 3/10 of the wavelength), the value of the transmission coefficient phase for the interior Sestroretskii cube equals the value of the SCHIE transmission coefficient phase. The value of the transmission coefficient phase is more dependent on the isolation quantity. Therefore, the influence on the transmission coefficient phase starts already from the isolation value equal to −34 dB (see Fig. 25).

Figure 26 shows the frequency characteristics of the estimate of delay time t during which the signal comes from input 2 to inputs 3–6 (curves 1–4) for the interior Sestroretskii cube. For the SCHIE, the frequency characteristics of the estimate of delay time t, during which the signal comes from input 2 to inputs 3 and 4 (curves 5 and 6), are given for comparison. It is seen from the figure that the time delay is 1.65 ps for inputs 3–6. The characteristic resonances of the delay time are seen at the frequencies of 150 GHz (when the size of the edge of the interior Sestroretskii cube corresponds to the half of the wavelength) and 300 GHz (when the size of the edge of the interior Sestroretskii cube corresponds to the wavelength).

Up to the frequency of 90 GHz (when the size of the edge of the interior Sestroretskii cube corresponds to 3/10 of the wavelength), the value of the estimate of delay time t of the signal transit for the interior Sestroretskii cube is close to the value of the estimate of the delay time of the signal transit for the SCHIE. When the frequency continues to increase, we observe
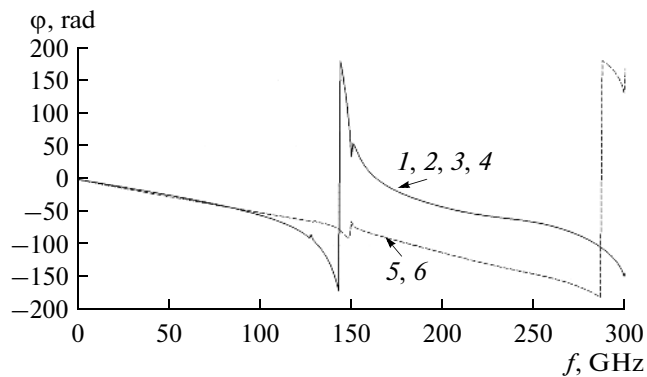

Fig. 25. Frequency characteristic of phase φ of the coefficient of transmission (curves 1–4) from input 2 to inputs 3–6 of the interior Sestrortskii cube and (curves 5 and 6) from input 2 to inputs 3 and 4 for the SCHIE.
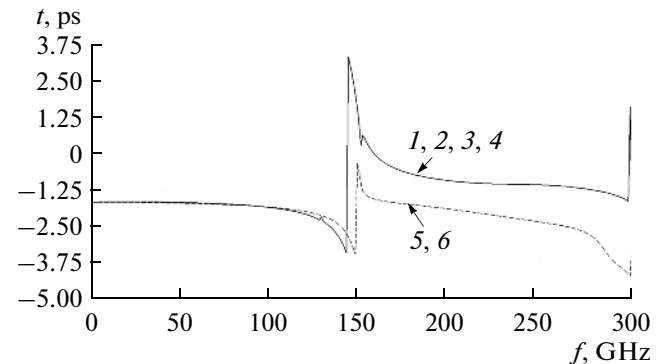

Fig. 26. Frequency characteristic of the time delay estimate for the signal propagating from (curve 1–4) input 2 to inputs (3–6) of the interior Sestrortskii cube and from (curves 5 and 6) input 2 to inputs 3 and 4 for the SCHIE.
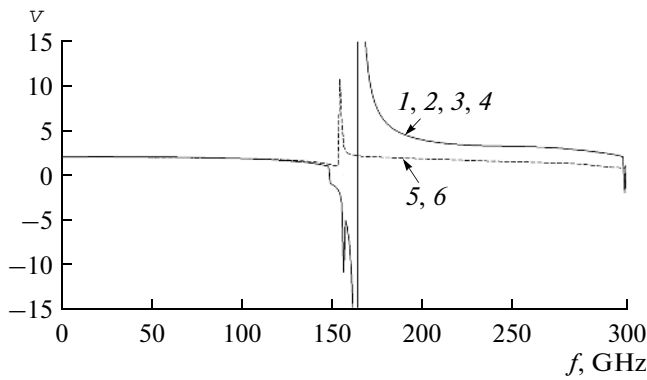
Fig. 27. Velocity of the signal transmission from (curve *1–4*) input *2* to inputs (*3–6*) of the interior Sestrortskii cube and from (curves *5* and *6*) input *2* to inputs *3* and *4* for the SCHIE.

substantial differences between the values of the estimate of the delay time of the signal transit for the interior Sestroretskii cube and the estimate of the delay time of the signal transit for the SCHIE. This corresponds to the behavior of the transmission coefficient phases (see Fig. 25).

The frequency characteristic of the velocity of signal transit from input *2* to inputs *3–6* (curves *1–4*) for the interior Sestroretskii cube is presented in Fig. 27. For comparison, the frequency characteristic of the velocity of the signal transit from input *2* to inputs *3* and *4* (curves *5* and *6*) for the SCHIE is also shown. It is seen from the figure that, at the frequency of 1 GHz, the value of the signal transit velocity in the interior Sestroretskii cube is twice as large as the light speed. After that, we observe the smooth decrease of the signal transit velocity to 0.97 of light speed *c* at the frequency of 142 GHz. At the frequencies of 150 and

300 GHz, we see the characteristic resonances of the signal transit velocity.

The value of the signal transit velocity for the interior Sestroretskii cube is close to the value of the signal transit velocity for the SCHIE up to the frequency of 100 GHz (when the size of the edge of the interior Sestroretskii cube corresponds to 1/3 of the wavelength). When the frequency continues to grow, these velocities are substantially different, which corresponds to the behavior of the phases of the transmission coefficient (see Fig. 25).

Thus, the analysis of the above frequency characteristics of the interior Sestroretskii cube enables us to make the following conclusions that confirm the positions formulated earlier in works [4–12].

(i) The considered interior Sestroretskii cube is described rather well in the one-mode approximation and exhibits the properties of a double waveguide T-branch [14] for the frequency as high as 100 GHz (when the dimension of the edge is 1/3 of the wavelength).

(1) Input *2* is matched and decoupled with input *1*.

(2) All the energy coming to input *2* is divided in the identical proportion between inputs *3–6*.

(3) When the amplitudes of the electric and magnetic field intensities of the wave incident on input *2* are taken as unity, the amplitudes of the waves arriving at inputs *3–6* will be equal to 1/2.

(4) When the amplitude of the vector of the power flux density of the electromagnetic wave incident on input *2* is equal to unity, the amplitudes of the power flux densities of electromagnetic waves reaching inputs *3–6* are equal to 1/4.

Figure 28 illustrates the directions of the vectors of the electric ($\vec{E}$) and magnetic ($\vec{H}$) fields and vectors of the flux densities of the waves incident on input *2* and
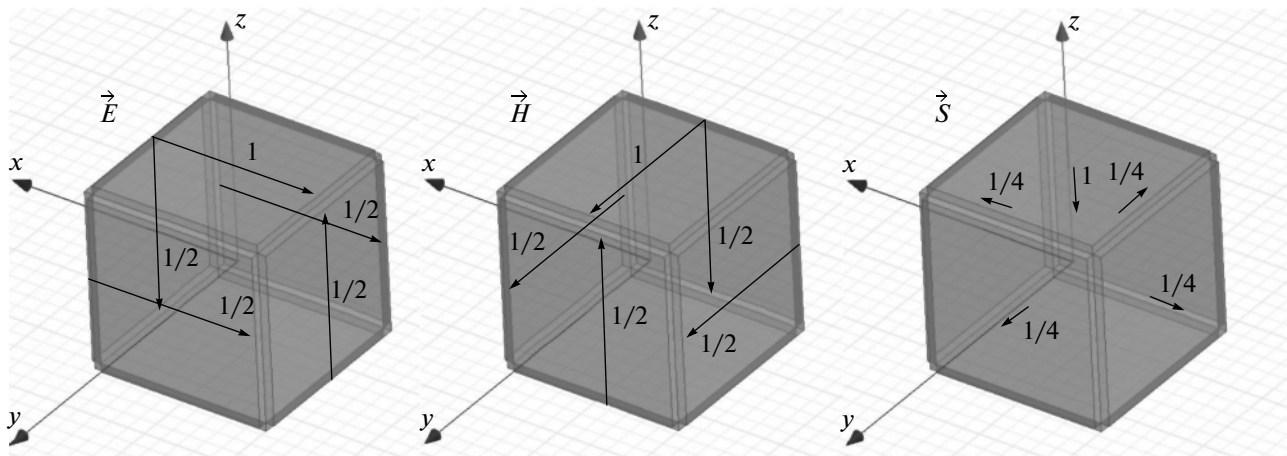

Fig. 28. Picture of the directions of the vectors of the electric ($\vec{E}$) and magnetic ($\vec{H}$) field intensities and of the vectors of the flux density of the waves incident on input *2* and coming to inputs *3–6* of the interior Sestrortskii cube.

coming to inputs *3–6* of the interior Sestroretskii cube.

(ii) When a monochromatic signal comes from input *2* to inputs *3–6*, the phase retard linearly depends on the frequency up to 100 GHz (when the size of the edge of the interior Sestroretskii cube corresponds to 1/3 of the wavelength). The corresponding delay time of the signal going from input *2* to inputs *3–6* does not depend on the frequency up to 100 GHz and corresponds to the doubled light speed in vacuum. This fact makes us possible to conclude that signals (including video pulses) whose spectrum lies in the band of up to 100 GHz go from input *2* to inputs *3–6* of the interior Sestroretskii cube with the velocity that is twice as large as the light speed in vacuum.

CONCLUSIONS

Numerical modeling has been performed in electrodynamic code ANSYS HFSS v.15 for the frequency characteristics of the interior Sestroretskii cube. It has been shown that the interior Sestroretskii cube has the properties of a double waveguide T-branch for wavelengths exceeding 1/3 of the edge length of the interior Sestroretskii cube. The hypothesis of works [4–7] that signals go from input *2* to inputs *3–6* of the interior Sestroretskii cube with the velocity that twice exceeds the light speed in vacuum has been confirmed. However, this is possible under the condition the their spectrum lies in the frequency band bounded by the frequency equal to 1/3 of the length of the edge of the interior Sestroretskii cube.

REFERENCES

1. A. S. Godin, A. B. Tsai, and K. N. Klimov, J. Commun. Technol. Electron. **60**, 329 (2015).
2. A. S. Godin, A. B. Tsai, and K. N. Klimov, J. Commun. Technol. Electron. **60**, 436 (2015).
3. A. S. Godin, A. B. Tsai, and K. N. Klimov, J. Commun. Technol. Electron. **60**, 737 (2015).
4. B. V. Sestroretskii and Yu. K. Vladimirov, *Computer-Aided Design of Devices and Microwave Systems* (O-vo "Znanie" USSR, Kiev, 1974), Part 1 [in Russian].
5. B. V. Sestroretskii, Vopr. Radioelektron., Ser. Obshchetekhn., No. 2, 113 (1976).
6. B. V. Sestroretskii, in *Interuniv. Collection Sci. Works "Machine Design of Devices and Microwave Systems"* (MIREA, Moscow, 1977), p. 127 [in Russian].
7. B. V. Sestroretskii, Vopr. Radioelektron., Ser. Obshchie Voprosy Radioelektron., No. 5, 56 (1983).
8. P. B. Johns, IEEE Trans. Microwave Theory Tech. **35**, 370 (1987).
9. W. Hoefer, IEEE Trans. Microwave Theory Tech. **33**, 882 (1985).
10. *The Transmission-Line Modelling Method: TLM* (Wiley-IEEE Press, New York, 1996).
11. V. Trenkič, "The development and characterization of advanced nodes for the TLM method," PhD Thesis (Univ. Nottingham, Nottingham, 1995).
12. P. Russer, Electromagnetics **16**, 537 (1996).
13. S. E. Bankov, V. D. Kurushin, and E. M. Guttsait, *Computation of Optical and Microwave Problems with Help HFSS* (Orkada, Moscow, 2012) [in Russian].
14. D. M. Sazonov, A. N. Gridin, and B. A. Mishustin, *Microwave Circuits* (Vysshaya Shkola, Moscow, 1981; Mir, Moscow, 1982).
15. K. N. Klimov, D. S. Gezha, and D. O. Firsov-Shibaev, *Practical Application of Electrodynamic Modelling* (Lambert Academic Publishing, Saarbrucken, 2012) [in Russian].
16. K. N. Klimov, D. O. Firsov-Shibaev, and D. S. Gezha, *Method of Impedance Analysis of Electromagnetic Space* (Lambert Academic Publishing, Saarbrücken, 2013) [in Russian].
17. G. T. Markov and D. M. Sazonov, *Antennas* (Energiya, Moscow, 1975) [in Russian].
18. S. I. Baskakov, *Bases of Electrodynamics* (Sovetskoe Radio, Moscow, 1973) [in Russian].
19. M. A. Zheksenov and A. S. Petrov, J. Commun. Technol. Electron. **59**, 289 (2014).
20. M. A. Zheksenov and A. S. Petrov, J. Commun. Technol. Electron. **59**, 427 (2014).
21. N. N. Fedorov, *Fundamental Electrodynamics* (Vysshaya Shkola, Moscow, 1980) [in Russian].
22. B. A. Vvedenskii and A. G. Arenberg, *Radio Waveguides* (Gostekhteorizdat, Moscow, 1946), Part 1 [in Russian].

Translated by I. Efimova